Design and analysis of an integrated driver for piezoelectric actuators

Mario Lok, David Brooks, Robert Wood, Gu-Yeon Wei
School of Engineering and Applied Sciences, Harvard University, Cambridge, MA, USA

***Abstract*— Small-scale, highly maneuverable, flapping-wing robotic insects have a wide range of applications, including exploration, environmental monitoring, search and rescue, and surveillance. For these small-scale robots, a piezoelectric cantilever actuator driven by a high voltage drive signal is a preferred actuation mechanism. The generation of this drive signal via light and efficient power electronics is critical given the limited weight budget for the flapping-wing robot. Previous work demonstrated actuator drive circuitry using discrete power transistors and passive elements. This paper presents a new design that integrates all the power FETs into a single monolithic IC, reducing the weight of the power electronics to fit within the weight budget. This design adds the capability of driving multiple outputs to accommodate recent electro-mechanical design advances for flying robots.**

I. INTRODUCTION

Developing a fully autonomous flapping-wing robotic insect at the sub-gram scale is a significant engineering milestone. Reaching this milestone enables many opportunities in environmental monitoring, search and rescue, and mobile sensor network deployment.

Recently, the Harvard Microrobotics Lab has demonstrated a flying robotic insect named "RoboBee" hovering and maneuvering along three axes, with bench-top high voltage amplifiers driving two piezoelectric actuators [1]. For full autonomy, the robot requires a battery, and power electronics that drive the actuators off of the battery. Furthermore, this robot must carry the power electronics and the battery within a combined payload weight budget, beyond which the robot cannot fly. Upon meeting the weight budget, further weight reductions improve flight time by allowing a larger battery [2]. Hence, the mass of the power electronics is an important design constraint.

In addition to being lightweight, the power electronics must meet the high operating voltage (~200V) and low operating frequency (~100Hz) requirements set by the actuators. Each actuator in the RoboBee consists of two piezoelectric layers attached to two sides of a fiberglass layer, shown in Fig. 1. It needs a high voltage supply (VDDH), a ground reference (GND), and a sinusoidal drive signal (VACT) for actuation. The high voltage supply and the ground reference are connected to the two piezoelectric layers while the middle fiberglass layer connects to the drive signal. The sinusoidal drive signal creates a periodic electric field across the two piezoelectric layers and causes the cantilever to produce an oscillatory motion, translating to wing flapping. The flapping amplitude is positively related to the lift force produced and proportional to the voltage amplitude of the drive signal. For a given drive-signal amplitude, the actuator produces the maximum amount of lift when the drive signal is a single tone sinusoidal waveform at the mechanical natural frequency of the wings [3], close to 100Hz. Electrically, each piezoelectric layer presents a mostly capacitive load to the power electronics. An accurate model of the actuator, comprising a nonlinear capacitor and a resistor in parallel, has been derived through experiments in previous work [4].

Given the weight budget and the characteristics of a piezoelectric actuator, an earlier implementation used a two-stage inductor-based design for a single actuator robotic insect, utilizing low profile inductors, discrete power switches in small packages, and a Kapton flexible PCB [5]. The use of an inductor for recovering energy from the capacitive load is a common theme shared by other piezoelectric actuator driver designs [6]. This initial driver circuit weighs 90mg, which was a significant improvement in density compared to a bench top high voltage amplifier.

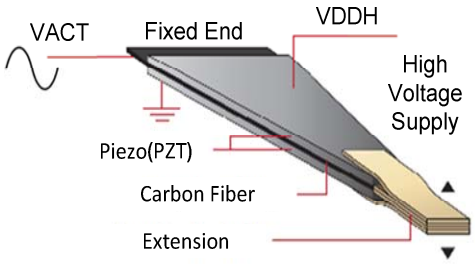

Fig. 1: Drawing of the piezoelectric actuator used in the RoboBee illustrates the mechanical design and electrical connections**.**

978-1-4799-0336-8/13/$31.00 ©2013 IEEE

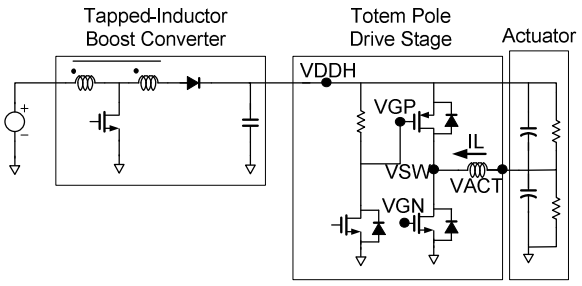

Fig. 2: This work adopts the two-stage power electronics topology from [5].

Since a maneuverable robotic insect requires two or more actuators, the naïve solution is to simply scale up the previous design to drive multiple outputs. However, the power supply for such a design would exceed our weight budget. One way to further improve driver density is to build it into a monolithic integrated circuit. In this work, we adopt the two-stage driver topology from [5], and place all of the power transistors on a single-die integrated circuit. As shown in Fig. 2, the tapped-inductor boost converter up-converts the 3.7V, supplied by the battery, to produce a constant high voltage supply VDDH, while the totem pole drive stage generates the large-swing drive signal for the actuator.

Our design targets a 500mg robot, and the corresponding weight breakdown is shown in Fig. 3. The combined payload budget for the power electronics and battery is 200mg. To generate 500mg of lift, the appropriate actuator size corresponds to two 22nF capacitive loads on the power electronics.

In contrast to prior work that demonstrate integrated piezoelectric actuators drivers with operating voltages at 50V and 80V [8][9], this paper focuses on the unique design challenges associated with integrating a totem drive stage circuit for higher actuator voltage levels. The parasitic capacitance in a higher voltage integrated circuit process is larger, which in turn impacts the operation of the totem pole drive stage. To mitigate issues associated with large parasitic capacitance, this work proposes two circuit techniques and analyzes the resulting benefit of an integrated design in terms of weight. Section II describes the circuit operation of the totem pole drive stage and analyzes the impact of large parasitic capacitances. Section III then describes the two circuit techniques that mitigate this impact. Lastly, Section IV presents a silicon prototype and experiments that validate the circuit technique and evaluate the power consumptions of an integrated driver design. The comparison between the integrated design and a scaled discrete design in flight time summarizes advantages of an integrated design.

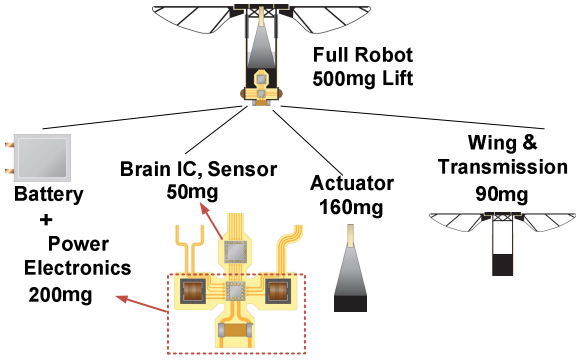

Fig. 3: The RoboBee consists of a battery, power electronics, brain IC, sensors, actuators, and wings connected to a mechanical transmission. The combined weight budget for battery and power electronics is 200mg.

II. Driver Design and Analysis

Flight time of the robot mostly depends on battery size and power consumption of the power electronics, specifically the efficiency of the boost stage and power consumption of the drive stage. To minimize drive stage power consumption, we can optimize transistor sizes, inductor size, and the control scheme to maximize the efficiency of energy delivery to the actuators and energy recovery from the actuators.

In this section, we transform the totem pole drive stage into simple, well-understood, equivalent circuit topologies, such as buck and boost converters, to facilitate efficiency optimization. Then, we consider two control schemes for the totem pole drive stage to improve power consumption. Finally, we analyze how parasitic capacitances in integrated DMOS transistors impact the operation of the totem pole drive stage.

A. Totem pole drive stage design

The totem pole drive stage must be capable of generating a sinusoidal drive signal, oscillating between the high voltage bias VDDH and ground reference GND. As shown in Fig. 2, the drive stage consists of a high-side transistor, a low-side transistor, an output inductor, and pre-driver circuitry for both the high-side and low-side transistors. The node that connects the high-side and low-side transistors is commonly referred to as the switch node (VSW). At the output, the drive stage sees large capacitive loads from the actuators between VDDH and VACT as well as between VACT and GND. The voltage at the VACT node is commonly referred to as the actuator voltage.

Fig. 4 illustrates the equivalent buck and boost converter topologies inherent to the totem pole driver depending on whether the actuator voltage is rising or falling. When the actuator voltage is rising, the high-side transistor and body diode of the low-side transistor form a voltage converter

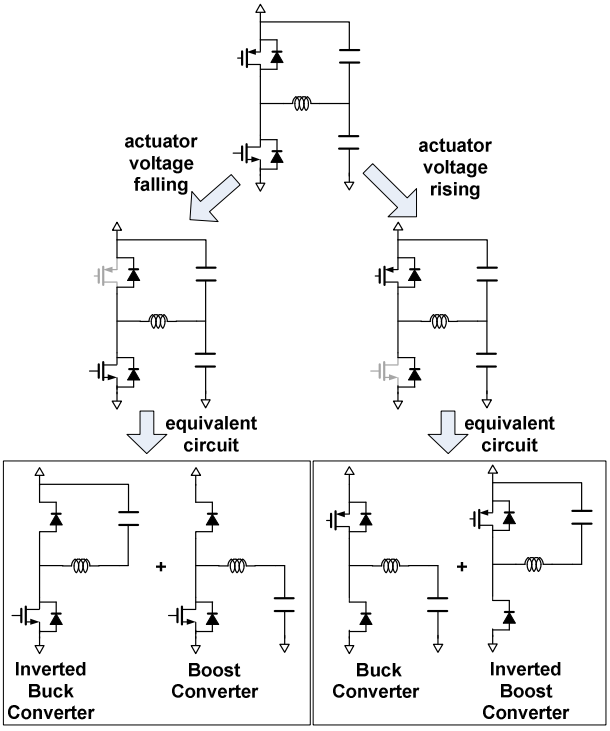

Fig. 4: Transforming the totem pole drive stage to equivalent circuit topologies facilitates efficiency analysis.

that raises the VACT node while the low-side transistor is always off. As illustrated in Fig. 4, the drive stage effectively acts like an inverted boost converter as it recovers energy from the top capacitive load. At the same time, it acts like a buck converter while delivering energy to the bottom capacitive load. Conversely, when the actuator voltage is falling, only the low-side transistor and body diode of the high-side transistor are used. Energy is delivered to the top load while it is being recovered from the bottom load. The equivalent circuit in this case is a combination of an inverted buck and boost converter.

In one energy conversion cycle, either transistor turns on for a predetermined amount of time, delivering energy to one capacitive load while withdrawing energy from the other. This results in a small change in the actuator voltage, VACT. A combination of the energy converted in each cycle and the timing between successive energy conversion cycles determines the slew rate of the drive signal.

An advantage of transforming the drive stage to the equivalent buck converter and boost converter is that the dependence of energy conversion efficiency on actuator voltage becomes obvious. The efficiency of energy delivery and recovery are optimized at each actuator voltage level by choosing the appropriate transistor on-time that minimizes switching and conduction losses.

B. Totem pole drive stage control

Although it is possible to use feed-forward control to pre-compute the off-time between energy conversion cycles, thus ensuring actuator voltage tracks a reference waveform, using feedback control guarantees more robust operation. One way to implement feedback control is to constantly compare the actuator voltage to the reference. When the actuator voltage trails behind the reference, the controller initiates an energy conversion cycle. Since the actuator oscillates slowly (100Hz) compared to the frequency of energy conversion cycles (~200KHz), the controller typically operates the drive stage in deep discontinuous conduction mode (DCM).

Alternatively, the controller can also operate in burst mode, initiating bursts of energy conversion cycles to adjust actuator voltage. One characteristic of burst mode operation is that the resulting actuator voltage waveform is a coarser approximation of the reference waveform with lower resolution. While deep DCM operation offers better drive signal quality over burst-mode operation, burst mode operation can help reduce power consumption of the drive stage. Moreover, experiments later show that degradation in drive signal quality has little impact on lift forces produced by the wings due to filtering via the mechanical transmission system.

C. Integrated DMOS implementation

Based on the discussions above, we now turn our attention to an integrated DMOS implementation for the power electronics. The monolithic solution offers opportunities to reduce mass, but introduces design challenges resulting from a totem pole drive stage implemented with integrated DMOS power transistors.

Integrated DMOS technology enables a lighter driver circuit than can be designed using discrete components. The minimum weight of a discrete power transistor chip in an SOT23 package is 8mg. In contrast, a minimum-sized integrated 300V transistor weighs 0.6mg, occupying 0.3mm^2 of die area 750µm thick. The flexibility in transistor sizing is an additional advantage of integrated designs.

However, integrated lateral DMOS transistors have much higher drain-to-source capacitance (C_{DS}) than discrete vertical power transistors do for equivalent saturation current, I_{SAT}, and on-resistance, R_{ON}. The larger C_{DS} comes

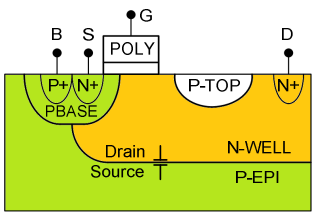

Fig. 5: DMOS cross section illustrates the reason for larger C_{DS} capacitance in an integrated process [10].

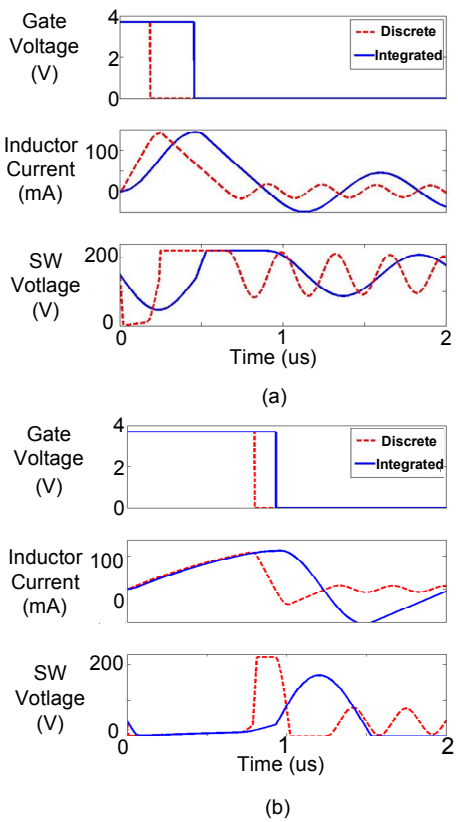

Fig. 6: Simulations of drive stage energy conversion cycles demonstrate the impact of large C_{DS}: (a) Large C_{DS} causes the transistor to remain in saturation, acting more like a current source than a switch. (b) Large C_{DS} causes the diode to not turn on for some actuator voltage levels.

from the large diffusion region between the drain-connected N-well and the source-connected P-substrate and P-base in the device structure, as shown in Fig. 4. Moreover, this diffusion area depends on breakdown voltage requirements. Thus, the C_{DS} capacitance is larger for a 200V device compared to that of a 50V device.

Larger C_{DS} not only increases switching losses in the energy conversion process, but it also alters drive stage operation in two different ways. Fig. 6 illustrates these changes via simulation traces of the gate voltage (VGN), inductor current (IL), and switch node voltage (VSW) during an energy conversion cycle. These plots compare operation of an integrated-transistor based design to a discrete-transistor based design.

The first change to drive stage operation is that C_{DS} prevents the transistor from fully turning on when the initial V_{DS} voltage (VSW) is large. As the transistor switches on, the large C_{DS} capacitance can hold the transistor in saturation such that the integrated transistor behaves more like a current source than a resistive switch.

In the example shown in Fig. 6(a), both the initial switch node voltage and the actuator voltage start out at 150V. For the simulation trace with integrated power transistors, as the low-side transistor turns on, the switch node voltage drops and reaches a minimum of 70V. Since 70V is still much higher than the V_{DSAT} of the transistor, the transistor behaves like a current source during the entire on-time. In comparison, voltage drops below V_{DSAT} when discrete power transistors are used.

The significance of this change is that the totem pole drive stage now has an additional mode of operation, where the inductor current and switch node voltage of the drive stage have a sinusoidal time dependence following Eqs. 1 and 2.

$$\boldsymbol{I_L = I_{SW} - I_{SW}\cos\left(\frac{1}{\sqrt{LC}}t\right)} \quad (1)$$

$$\boldsymbol{V_{SW} = V_{INIT} - \left(\sqrt{\frac{L}{C}} * I_{SW}\right)\sin\left(\frac{1}{\sqrt{LC}}t\right)} \quad (2)$$

The condition for the power transistor to remain in saturation is when the initial switch node voltage V_{INIT} satisfies the inequality in Eq. 3. In this new mode of operation, energy loss in the transistor can be computed by integrating the product of switch node voltage and transistor current via Eq. 4, which further reduces to Eq. 5. This equation computes energy loss in the transistor more accurately than Eq. 6, which underestimates loss by assuming the transistor operates as a switch.

$$\boldsymbol{V_{INIT} > V_{DSAT} + \left(\sqrt{\frac{L}{C}} * I_{SW}\right)} \quad (3)$$

$$\boldsymbol{E_{loss} = \int_0^{t_{ON}} I_{SW} V_{SW}\, dt} \quad (4)$$

$$\boldsymbol{E_{loss} = I_{SW}\left(V_{init}\, t_{ON} - L I_{PEAK}\right)} \quad (5)$$

$$\boldsymbol{E_{loss} = \frac{1}{2} I_{SW}^2 R_{ON} t_{ON} + \frac{1}{2} C_{DS} V^2} \quad (6)$$

Another important takeaway from Eq. 5 is that the actuator control scheme should maximize peak inductor current, I_{PEAK}. For the small inductor used in our application, the core saturation limit sets this peak inductor current. The control parameter, on time (t_{ON}) can be computed from Eq. 1 by substituting I_{LMAX} for I_L.

The second change to drive stage operation is seen during the rectifying phase of a conversion cycle. After the power switch turns off, energy stored in the inductor cannot sufficiently charge/discharge the C_{DS} capacitance and turn on the rectifying diode for parts of the actuator drive signal sinusoid. Hence, energy conversion efficiency is lower with no energy recovery.

Fig. 6(b) illustrates an example in which the energy in the inductor is not sufficient to slew the switch node to reach the 200V supply voltage for an integrated design. As a result, the body diode of the high-side switch is not turned on. The consequence is less energy, drawn from the bottom load, is recovered to the input.

In summary, the two aforementioned changes to drive stage operation cause the drive stage to suffer more losses than just higher $1/2C_{DS}V_{ACT}^2$ switching loss. The efficiency loss due to transistors remaining in saturation is high for large initial voltages across the transistor. At the same time, the loss due to the diode not turning on is high for large initial voltages across the rectifying diode. Since the high supply bias VDDH is a sum of the initial transistor voltage and the diode voltage, C_{DS}-dependent losses scale with VDDH.

Simulations of resulting energy delivery and recovery efficiencies are shown in Fig. 7 for a 200V totem pole drive stage. The efficiencies of a drive stage with an output inductor are compared to a design without an output inductor. Given the symmetry in the drive signal, only the half cycle when actuator voltage is falling is considered.

The simulation results show that when the actuator voltage is larger than 100V, the drive stage design with an inductor has better energy delivery efficiency and has higher than 50% energy recovery efficiency. The losses associated with the transistor remaining in saturation limit efficiency in this actuator voltage range. As actuator voltage reduces below 100V, the initial voltage across the diode becomes increases and the C_{DS} capacitor requires more energy from the inductor. When the actuator voltage falls to 70V, residual energy in the inductor cannot turn on the diode. In this actuator voltage range, the energy delivery efficiency of an inductor-based drive stage is identical to an inductor-less design and the energy recovery efficiency is negative.

In addition to serving as a comparative reference for the inductor-based drive stage design, the inductor-less drive stage is also a design candidate. Since each inductor consumes 15mg, we can trade lower efficiency for weight reduction and assess this additional design point in overall terms of overall weight and flight time.

D. C_{GD} Miller Capacitance Problem

In addition to the C_{DS} capacitance, C_{GD} Miller capacitance also impacts drive stage operation. During the drive signal phase in which the actuator voltage is falling, the switch node voltage abruptly falls in response to the transistor switching on. This large voltage swing on VSW can couple through the C_{GD} of the high-side transistor to the gate of the high side transistor. If the gate of the high side transistor is not driven with sufficiently low impedance, the high side switch can inadvertently conduct while the low-side transistor is still on, causing the drive stage to draw additional DC current and increase loss.

This problem was not anticipated in our design, because the C_{GD} capacitance turned out to be much larger than predicted by the transistor models. In order to work around this problem during testing, we replaced the P-type transistor in the topology shown in Fig.2 with an N-type transistor that was also integrated onto the die. The gate of this high-side N-type transistor is driven by a discrete, off-chip, low-impedance floating pre-driver.

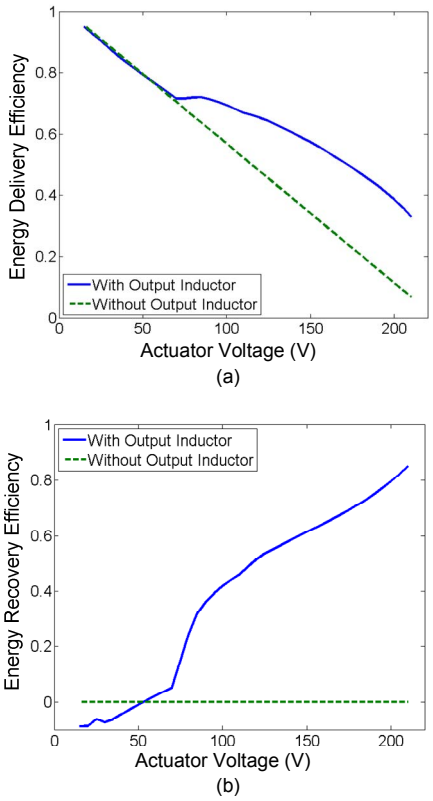

Fig. 7: Energy delivery and recovery efficiency for initial actuator voltages ranging from 0 to 200V shows the limitations of integrated drive stage power consumption.

III. Circuit Techniques

In light of the limitations that large C_{DS} capacitance imposes on the totem pole drive stage, this section describes two circuit techniques to reduce its power consumption.

A. Boosted gate driver

We implemented a simple circuit to boost the gate drive voltage for the low-side transistor to the maximum voltage allowed. Although the input battery voltage is 3.7V, the power transistors fully turns on at 5V and safely operates up to 8V. The additional switching power resulting from large gate drive voltages is a small fraction of the total power, because it is still much smaller than the voltage swing on the drain. Moreover, for the same saturation current, a higher gate drive voltage allows for smaller transistor size, smaller C_{DS} capacitance, and lower overall power

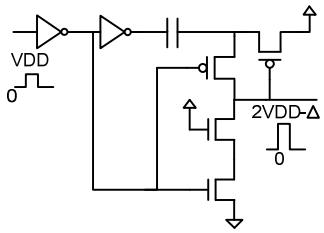

Fig. 8: A boosted gate driver generates a gate drive signal that is close to two times the input signal.

consumption. Fig. 8 presents a schematic of boosted gated driver circuit. For an input voltage pulse of 0-3.7V, this circuit generates an output voltage pulse of 0-6V without requiring an additional 6V supply voltage.

B. Voltage-valley switching in burst-mode operation

Soft switching is often used to address the energy loss problem associated with large $C_{DS.}$ Voltage-valley switching is a technique that turns on the power transistor when the drain source voltage is at its minimum (i.e., valley). In the totem pole drive stage design, when an energy conversion cycle completes, the residual energy in the inductor and the switch node capacitor causes the VSW to oscillate at a frequency of approximately $1/\sqrt{LC}$. Subsequent conversion cycles can exploit this oscillation by scheduling the instant at which the gate turns on to coincide with the instant at which the drain source voltage across the transistor is at its local minimum. Although the switching loss remains high for the first energy conversion cycle, subsequent cycles can benefit from voltage-valley switching to minimize switching losses. It is only possible to exploit the residual LC oscillation when subsequent energy conversion cycles are close in time. Otherwise, the oscillation of the switch node voltage cause by an earlier conversion cycle would have been damped out by the series resistance of the inductor by the time a later conversion cycle starts. Therefore, voltage-valley switching requires burst-mode operation.

A side effect of burst-mode operation is that large amounts of energy are delivered to the output followed by long idle periods. This leads to actuator drive signals that exhibit larger, coarse-grained steps compared to non-burst mode operation. As the number of burst cycles increases, the approximation becomes coarser and the resultant drive signals have lower resolution. A lower resolution drive signal generally does affect actuator motion and the force generated from actuation. However, our experiments show that lift forces measured on an actual flying robot suffer almost no degradation across a wide range of drive signal resolution. The details of this experiment and the findings are shown in Section IV-C.

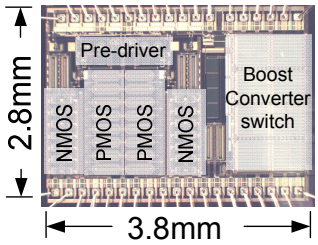

Fig. 9 The silicon die photo shows different components of the integrated design.

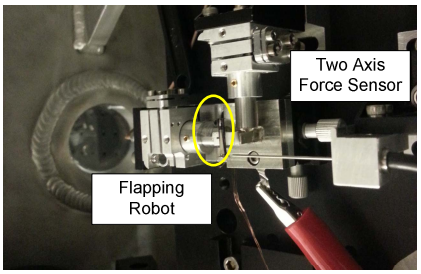

Fig. 10 A two-axis force sensor measures the lift force generated from the flapping motion of a half robot.

IV. PROTOTPE AND RESULTS

Power electronics for the flapping-wing actuators was implemented in a DALSA 0.8um 300V DMOS process. This test-chip prototype implements a transistor switch for the tapped-inductor boost converter, feedback circuitry for the boost converter, and two totem pole drive stage circuits, as shown in the die photo in Fig. 9. We conducted two experiments to quantify the side effects of burst-mode operation and measure the power consumption of the integrated power electronics for flapping-swing actuation. Based on power consumption and weight of the prototype, different drive stage designs are then compared.

A. Lift force vs. drive signal resolution experiment

Burst-mode operation reduces drive stage power consumption, but produces lower resolution drive signals. However, any degradation in lift force due to the lower resolution drive signal will offset improvements in power consumption. Thus, we first quantify the impact of drive signal resolution on lift force.

The lift force measurement setup comprises one half of the robotic insect mounted on a two-axis force sensor as shown in Fig. 10. This half piece includes one actuator, a transmission frame, and a wing. To characterize the actuator's dependence on driving waveform precision, both quantitative and qualitative, the vertical component of the two-axis force sensor logs the lift force generated from wing flapping and a high-speed camera records wing motion.

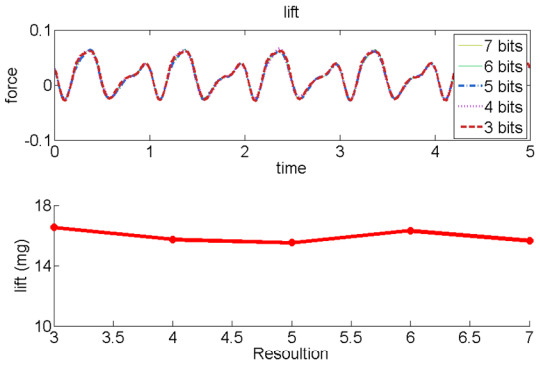

Fig. 11: Lift force measurements show lower-resolution drive signals have little impact on lift.

As shown in Fig. 11, both the time-dependent force measurements and the average lift measurements shows that when the actuator is driven at 100Hz, lift force exhibits little change as drive signal resolution changes from 7 bits down to 3 bits. The peak-to-peak difference in lift force is less than 2%, some of which can be attributed to measurement noise. Video capture of wing motion corresponding to sine waves with 7 and 3 bits of resolution also look identical. A lower precision drive signal does not impact wing motion and lift force because the inertia of the wing and actuator low-pass filters high-order harmonic content in a low precision driving waveform. This is consistent with low-pass filtering behavior reported in previous studies [13].

To confirm this filtering effect, we tried reducing the drive signal frequency to 30Hz, below the resonance of the mechanical system. Although the lift force is too small for the measurement setup to obtain an accurate measurement, video captures clearly show erratic wing stroke when sine wave resolution falls below 5 bits.

Since the optimal drive signal frequency for the actuator in the robot is close to 100Hz, the results of this experiment indicates that burst mode operation can be applied in the drive stage with little penalty to lift.

B. Totum pole drive stage power measurement

To measure drive stage power consumption, we loaded the power electronics with a pair of 22nF capacitors that mimic the loading of the piezoelectric actuator. The experimental setup includes feedback circuitry for the totem pole drive stage implemented on a FPGA board and a custom PCB. An external 300V power supply replaced the first stage DC-DC converter to isolated power consumption of the second-stage totem pole driver.

Table 1 summarizes the measured power consumption for different totem pole drive stage configurations generating a 0-200V, 100Hz sinusoid. The previous discrete design consumes 120mW [1]. For the drive stage configuration with a P-type high-side transistor, the total power consumption is 181mW (initial measurement: 200mW)

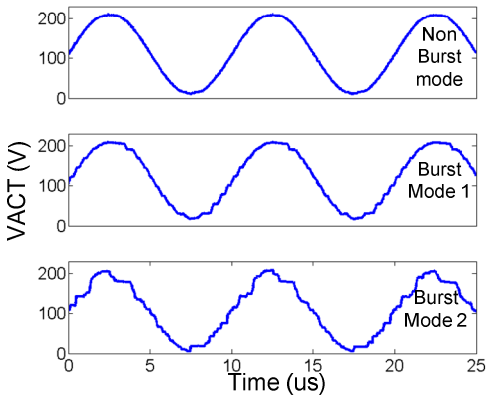

Fig. 12: Burst-mode operation produces lower-resolution drive signal sinusoids.

with an off-chip, 220µH output inductor and 190mW without the inductor. As mentioned previously, the topology with the inductor consumes higher power than predicted by simulation because of the C_{GD} Miller capacitance problem.

Table 1: Summary of drive stage power consumption.

Drive signal	0-200V, 100Hz
Actuator load	22nF x 2 layers
Discrete drive stage	120 mW
Integrated, w/ L, P-type high side	181 mW
Integrated, no L, N-type high side	190 mW
Integrated, w/ L, N-type high side	162 mW
Integrated, w/ L, N-type high side (burst 1)	153 mW
Integrated, w/ L, N-type high side (burst 2)	140 mW

To evaluate the benefits of burst-mode control and voltage-valley switching, we measured the power consumption of the drive stage design with an N-type high-side transistor. Even without burst mode, power consumption reduces to 162mW compared to using P-type high-side transistor due to lower switching, conduction, and C_{DS} capacitance losses. When two burst mode settings are applied, power consumption of the drive stage reduces to 153mW and 140mW. The first burst mode produces a drive signal that has more than 4 bits of resolution while the second burst mode reduces the resolution of the drive signal down to approximately 3 bits. Fig. 12 shows the drive signal obtained with and without burst mode.

C. Weight comparison

The die alone weighs 35mg. We estimate total power electronics weight to be 95mg by summing all component mass with assembly overhead, accounting for solder and flexible PCB board. We measured tapped-inductor boost converter efficiency equals 49% with an integrated switch, which is lower than the 75% efficiency possible for a design using discrete components. Hence, the 95mg total assumes a separate first stage and an integrated second stage.

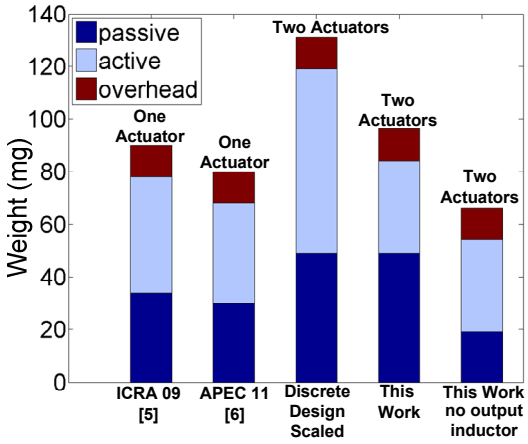

Fig. 13: Weight comparisons with different drive stage implementations show the advantages of an integrated design.

As shown in Fig. 13, we project an overall reduction of 35mg for a dual-actuator driver compared to scaling the original design built with discrete components. Eliminating the output inductor in the totem pole drive stage can reduce the overall weight by 65mg. Further weight reduction is possible by thinning the silicon die and cutting out unused edges.

For the totem pole drive stage design with an output inductor, the current integrated design is measured to have 50.8% higher power consumption. Since the power electronics and the battery have a combined weight budget of 200mg, a 35mg reduction in weight for the power electronics translates to a 50% larger battery. Assuming constant battery energy density, projected flight time remains constant. For the totem pole drive stage design without the output inductor, power consumption is 58.3% higher while 65mg weight reduction translates to a 92.8% larger battery and longer flight times.

V. CONCLUSION

This paper described a lightweight alternative for a piezoelectric actuator driver using integrated high voltage DMOS technology. A prototype with all power transistors implemented on a single die was shown. While the larger C_{DS} changes the way the totem pole drive stage operates and increases the power consumption, different actuator control schemes and circuit techniques can reclaim some of the power. Future designs that address the C_{GD} coupling issue can further reduce power consumption. We are also actively exploring alternative actuator designs and driver topologies to alleviate the negative effects of large C_{DS} and C_{GD} capacitance. Since the weight budget is a key design target, we are also exploring ways to eliminate the output inductors while maintaining high energy efficiency.

ACKNOWLEDGMENTS

The authors thank CMC Microsystems and DALSA semiconductor for foundry service. The authors also thank the Harvard Microrobotics Laboratory for thoughtful discussions and assistance with experimental measurements. This work was supported in part by the NSF Expeditions in Computing Award #: CCF-0926148.

REFERENCE

[1] K. Ma, et al. "Design, fabrication, and modeling of the split actuator microrobotic bee." *Intelligent Robots and Systems (IROS), 2012 IEEE/RSJ International Conference on*. IEEE, 2012.

[2] M. Karpelson, et al. "Energetics of flapping-wing robotic insects: towards autonomous hovering flight," *Intelligent Robots and Systems (IROS), 2010 IEEE/RSJ International Conference on.* IEEE, 2010.

[3] N. P´erez-Arancibia, et al. "First controlled vertical flight of a biologically inspired microrobot," *Bioinspiration & Biomimetics*, vol. 6, p. 036009, 2011.

[4] M. Karpelson, et al. "Driving high voltage piezoelectric actuators in microrobotic applications." *Sensors and Actuators A: Physical, 2012*.

[5] M. Karpelson, et al. "Milligram-scale high-voltage power electronics for piezoelectric microrobots," in *Robotics and Automation,2009. ICRA'09. IEEE International Conference on*. IEEE,2009.

[6] B. Edamana, Biju, and Kenn R. Oldham. "Optimal Low-Power Piezoelectric Actuator Control With Charge Recovery for a Microrobotic Leg." *Mechatronics, IEEE/ASME Transactions on* , IEEE, 2013.

[7] D. Campolo, et al. "Efficient charge recovery method for driving piezoelectric actuators with quasi-square waves," *Ultrasonics, Ferroelectrics and Frequency Control, IEEE Transactions on*. IEEE, 2003.

[8] P. Miribel-Català, et al. "Smart power integrated circuit for a piezoelectric miniature robot." *Analog Integrated Circuits and Signal Processing*. 2002.

[9] L. Fontanella, et al. "Single chip, self supplied, voltage and charge mode double 80V piezoelectric actuator driver," *Solid-State Circuits Conference,* 1999.

[10] J.-F.Richard, et al. "High voltage interfaces for CMOS/DMOS technologies." *the first IEEE Northeast Workshop on Circuits and systems, Montreal, Canada*. IEEE, 2003.

[11] YP Liu, D. Vasic. "Small power step-up converter for driving flapping wings of the micro robotic insects," *Energy Conversion Congress and Exposition (ECCE),* IEEE, 2012.

[12] A. Mesgarani, et al. "Supply boosting technique for designing very low-voltage mixed-signal circuits in standard CMOS," *Circuits and Systems (MWSCAS),* IEEE, 2010.

[13] B.M. Finio, et al. "System identification and linear time-invariant modeling of an insect-sized flapping-wing micro air vehicle," *Intelligent Robots and Systems (IROS),* IEEE, 2011.